Evolution of modular intraflagellar transport from a coatomer-like progenitor

Teunis J. P. van Dam[a], Matthew J. Townsend[b], Martin Turk[c,1], Avner Schlessinger[c,2], Andrej Sali[c,d,e], Mark C. Field[b,3], and Martijn A. Huynen[a,3,4]

[a]Centre for Molecular and Biomolecular Informatics, Radboud University Medical Centre, 6500 HB, Nijmegen, The Netherlands; [b]Department of Pathology, University of Cambridge, Cambridge CB2 1QP, United Kingdom; and [c]Department of Bioengineering and Therapeutic Sciences, [d]Department of Pharmaceutical Chemistry, and [e]California Institute for Quantitative Biosciences, University of California, San Francisco, CA 94158

Edited by Russell F. Doolittle, University of California at San Diego, La Jolla, CA, and approved March 15, 2013 (received for review December 4, 2012)

The intraflagellar transport (IFT) complex is an integral component of the cilium, a quintessential organelle of the eukaryotic cell. The IFT system consists of three subcomplexes [i.e., intraflagellar transport (IFT)-A, IFT-B, and the BBSome], which together transport proteins and other molecules along the cilium. IFT dysfunction results in diseases collectively called ciliopathies. It has been proposed that the IFT complexes originated from vesicle coats similar to coat protein complex (COP) I, COPII, and clathrin. Here we provide phylogenetic evidence for common ancestry of IFT subunits and α, β′, and ε subunits of COPI, and trace the origins of the IFT-A, IFT-B, and the BBSome subcomplexes. We find that IFT-A and the BBSome likely arose from an IFT-B–like complex by intracomplex subunit duplication. The distribution of IFT proteins across eukaryotes identifies the BBSome as a frequently lost, modular component of the IFT. Significantly, loss of the BBSome from a taxon is a frequent precursor to complete cilium loss in related taxa. Given the inferred late origin of the BBSome in cilium evolution and its frequent loss, the IFT complex behaves as a "last-in, first-out" system. The protocoatomer origin of the IFT complex corroborates involvement of IFT components in vesicle transport. Expansion of IFT subunits by duplication and their subsequent independent loss supports the idea of modularity and structural independence of the IFT subcomplexes.

complex modularity | molecular evolution

The eukaryotic cilium or flagellum is a structure protruding from the cell into the environment. The cilium provides motility by a controlled whip-like or rotational beating. Construction and maintenance of the cilium, together with additional signaling functions, depend on the process of intraflagellar transport (IFT). IFT provides active, bidirectional transport of proteins and other molecules along the length of the cilium, delivering structural components and other factors in the organelle. IFT dysfunction results in the inability of the cilium to maintain a normal structure and failure of signaling and sensory pathways, causing complex system-wide disorders and syndromes (1).

IFT is mediated by a large cohort of evolutionarily conserved subunits, which can be grouped by biochemical and genetic criteria into three subcomplexes: IFT-A, IFT-B, and BBSome. Broadly, mutations in any subunit of each of these complexes phenocopy each other, indicating close cooperativity and a requirement for complete holocomplexes for functional IFT. Significantly, six IFT complex subunits (WDR19, WDR35, IFT140, IFT122, IFT172, and IFT80) have predicted secondary structure elements and folds similar to those present in multiple subunits of vesicle coat complexes and the nuclear pore complex (NPC) (2–4). Their N-terminal region contains WD40 repeats, likely forming two β-propeller folds, whereas their C-terminal region contains tetratricopeptide repeats (TPR), likely forming an α-solenoid–like fold.

The IFT system has been shown to be homologous to the protocoatomer family of complexes, which includes coat protein complex (COP) I, COPII, clathrin/adaptin complex, and the NPC scaffold (2–4). This classification was based on sequence similarity of IFT subunits to the COPI-α and -β′ subunits, further supported by secondary structure predictions. However, a full phylogenetic reconstruction and structural analysis of the IFT complex has not been performed. Such an analysis is necessary because the abundance of the WD40 and TPR domains in non-coatomer subunit proteins requires more than sequence similarity to establish a close phylogenetic relationship. Here, we have reconstructed the evolution of the IFT complex in detail, and provide phylogenetic evidence that the IFT complex is indeed a sister structure to COPI. Analysis of the presence of the individual subcomplexes in currently living eukaryotes shows that the presence and inferred order of the loss of subcomplexes mirrors their origin—the IFT subcomplex that was added latest in evolution is the first to be lost.

Results

The known IFT system consists of three subcomplexes, IFT-A, IFT-B, and BBSome, together comprising 33 subunits in *Homo sapiens* ($n = 7$, $n = 17$, and $n = 10$, respectively). Twenty-one of these subunits can be divided into four groups based on homology relationships and predicted structures (Fig. 1*A*). The first group (Fig. 1*A*, blue) comprises WDR19, WDR35, IFT140, IFT122, IFT172, and IFT80, whose domain structure resembles COP-α and -β subunits (2–4) (as detailed later). For brevity, we will henceforth refer to these proteins as the αβ-IFT subunits. The second group (Fig. 1*A*, yellow) comprises TTC21, IFT88, TTC26, TTC30A/B, BBS4, and BBS8, whose domain structure resembles the COP-ε subunit and are henceforth referred to as ε-IFT subunits. The third group (Fig. 1*A*, red) comprises the small GTPases IFT22, IFT27, and BBS3. Finally, the fourth group (Fig. 1*A*, green) comprises BBS1, BBS2, BBS7, and BBS9, and represents four homologous subunits in the BBSome. The remaining IFT subunits (Fig. 1*A*, white) do not share any detectable sequence relationships with each other, or with any other proteins. Hence, as they do not contain any phylogenetic information on the origin of the IFT complex, they will not be further discussed. Interestingly, members of the four homologous groups

Author contributions: T.J.P.v.D., M.C.F., and M.A.H. designed research; T.J.P.v.D., M.J.T., M.T., and A. Schlessinger performed research; T.J.P.v.D., M.J.T., M.T., A. Schlessinger, A. Sali, and M.C.F. analyzed data; and T.J.P.v.D., M.T., A. Schlessinger, A. Sali, M.C.F., and M.A.H. wrote the paper.

The authors declare no conflict of interest.

This article is a PNAS Direct Submission.

Freely available online through the PNAS open access option.

[1]Present address: Gene Center and Center for Integrated Protein Science Munich and Department of Biochemistry, University of Munich, 81377 Munich, Germany.

[2]Present address: Department of Pharmacology and Systems Therapeutics and Tisch Cancer Institute, Mount Sinai School of Medicine, New York, NY 10029.

[3]M.C.F. and M.A.H. contributed equally to this work.

[4]To whom correspondence should be addressed. E-mail: huynen@cmbi.ru.nl.

This article contains supporting information online at www.pnas.org/lookup/suppl/doi:10.1073/pnas.1221011110/-/DCSupplemental.

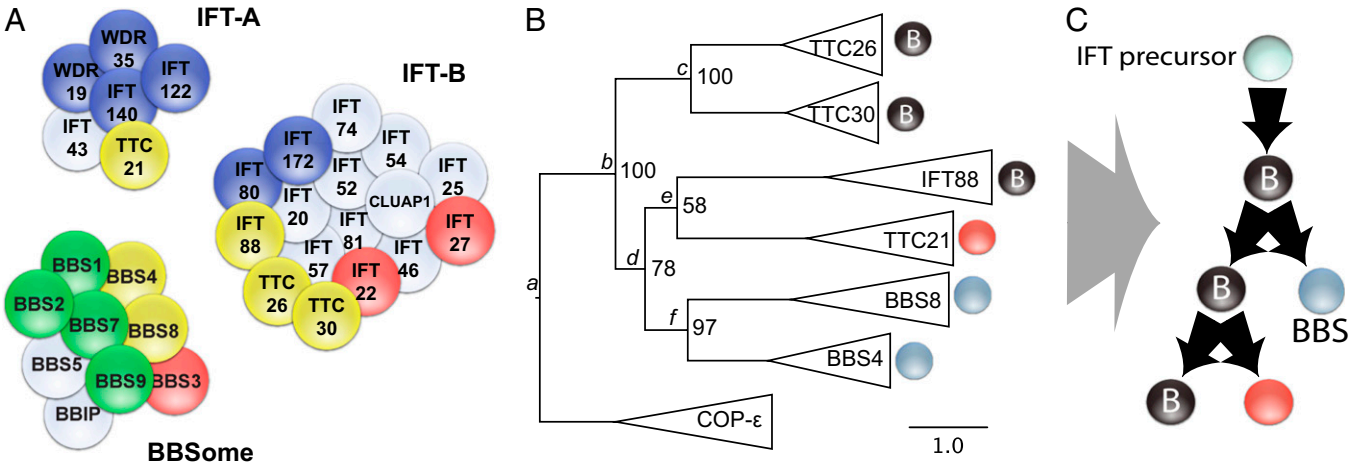

Fig. 1. Phylogenetic analyses of the ε-IFT subunits and IFT complex composition. (*A*) Composition of the IFT subcomplexes. Blue, αβ-IFT subunits with domain structures similar to COPI-α and -β′; yellow, ε-IFT subunits with domain structures similar to COPI-ε; red, small GTPases; green, putative β-propeller BBS subunits; white, subunits that are not homologous to other subunits. Positions of the subunits do not reflect their actual positions within the IFT complex. (*B*) Phylogenetic tree of ε-IFT subunits. (*C*) Evolutionary scenario for the origin of IFT-A, IFT-B, and BBSome subcomplexes, based on *B*.

are not confined to a specific subcomplex, indicating a convoluted origin of the three subcomplexes. Here we discuss two of these groups, the αβ-IFT and ε-IFT subunits, and report an evolutionary reconstruction of their origin. Discussions of the other two groups are provided in *SI Discussion*.

Common Descent of IFT and COPI-α, -β′, and -ε Subunits. Sensitive sequence similarity searches [i.e., hidden Markov models (HMMs) and PSI-BLAST] using the sequences of αβ-IFT subunits (Fig. 1*A*, blue) as queries retrieved many TPR- and WD40-containing protein sequences, including the α and β′ subunits of the COPI complex. However, none of these were retrieved consistently for all αβ-IFT subunits. This lack of consistency in detection of proteins that are most similar to the αβ-IFT subunits argues for a phylogenetic approach to identify the origin of the αβ-IFT subunits. Unfortunately, variability in the number and length of the WD40 and TPR domains within the αβ-IFT subunits prevents unambiguous alignment of these sequences. To overcome this, we searched for a common region of sequence similarity among the αβ-IFT subunits. We detected a region of ∼150 aa residues that lies between the β-propeller and α-solenoid–like segments in all αβ-IFT subunits, and that aligned consistently without the need to insert long gaps into the alignment (Fig. 2 and Fig. S1). Iterative similarity searches with the use of an HMM for this region resulted in the retrieval of all αβ-IFT subunits as well as, importantly, the α and β′ subunits of the COPI complex. No other significant hits where retrieved, strongly suggesting a common origin for the αβ-IFT and COPI-α and COP-β′ subunits.

For the ε-IFT subunits (Fig. 1*A*, yellow), we used an HMM vs. HMM search to determine whether the ε-IFT subunits are each other's closest paralogs and whether the COP-ε subunit indeed represents the closest non-IFT subunit relative. HMMs for each of the ε-IFT subunits and COP-ε were constructed and added to the complete set of HMMs of protein families in the Panther database (5). In most comparisons (Table S1), COP-ε and the ε-IFT subunits represent reciprocal best hits, suggesting that COP-ε is indeed the closest non-IFT paralog of the ε-IFT subunits.

We subsequently constructed multiple sequence alignments and phylogenetic trees for the αβ- and ε-IFT subunits. Importantly, inclusion of COP-α, COP-β′, and COP-ε sequences allowed us to root the phylogenetic trees and infer the order in which the individual αβ- and ε-IFT subunits originated. The topology of the ε-IFT phylogeny (Fig. 1*B*) suggests that the proto-IFT complex was IFT-B–like (the IFT-B subunits can be found in both clades originating in node *b*, whereas the BBSome and IFT-A subunits emerge later). BBSome subunits BBS4 and BBS8 originate from a duplication at node *d* followed by a duplication in node *f*, suggesting that the BBSome subcomplex emerged later in the proto-IFT complex. Duplication of the ancestral ε-IFT subunit at node *e* gave rise to IFT88 (IFT-B) and TTC21 (IFT-A), suggesting that the IFT-A subcomplex is the latest addition to the proto-IFT complex and completes the extant IFT system. Fig. 1*C* shows a cartoon representation of the sequence of subcomplex emergence.

The αβ-IFT phylogenetic tree is not fully resolved and supports two distinct evolutionary scenarios with respect to the order in which the subcomplexes originated (*SI Discussion* provides more details), one of which is congruent with the scenario for the ε-IFT subunits.

Loss of IFT Subcomplexes Reflects Modularity Within IFT Complex. The full IFT system is not retained in all eukaryotic species. In fact, cilium loss has occurred in multiple taxa, including Apicomplexa, most fungi, and seed plants (6, 7). To obtain a high-resolution picture of IFT presence and loss, we searched for orthologues of known IFT subunits in a selected set of 52 sequenced genomes of divergent eukaryotic species by using sensitive homology detection methods, including PSI-BLAST and HMMs (Fig. 3). We included ciliate and nonciliate species to determine the exclusiveness of IFT subunits to ciliated species. All the subunits reported for the human IFT complexes are conserved throughout the eukaryotic lineage. Therefore, IFT-A, IFT-B, and BBSome were likely present in the last eukaryotic common ancestor (LECA) and comprised all currently known IFT subunits from human and *Chlamydomonas reinhardtii*, in agreement with earlier observations (4, 7).

Despite the correlation between the presence of IFT subunits and the cilium, IFT subunits are not universally conserved in all ciliated species (Fig. 3). Most interesting is the loss of the BBSome in *Batrachochytrium dendrobatidis*, *Selaginella moellendorffii*, *Physcomitrella patens*, *Thalassiosira pseudonana*, and *Toxoplasma gondii* (*SI Discussion* provides a detailed description of these species). These species represent four independent lineages in eukaryotic evolution, and hence the losses represent separate events. Interestingly, all the species lacking the BBSome are closely related to species that have also lost the entire cilium

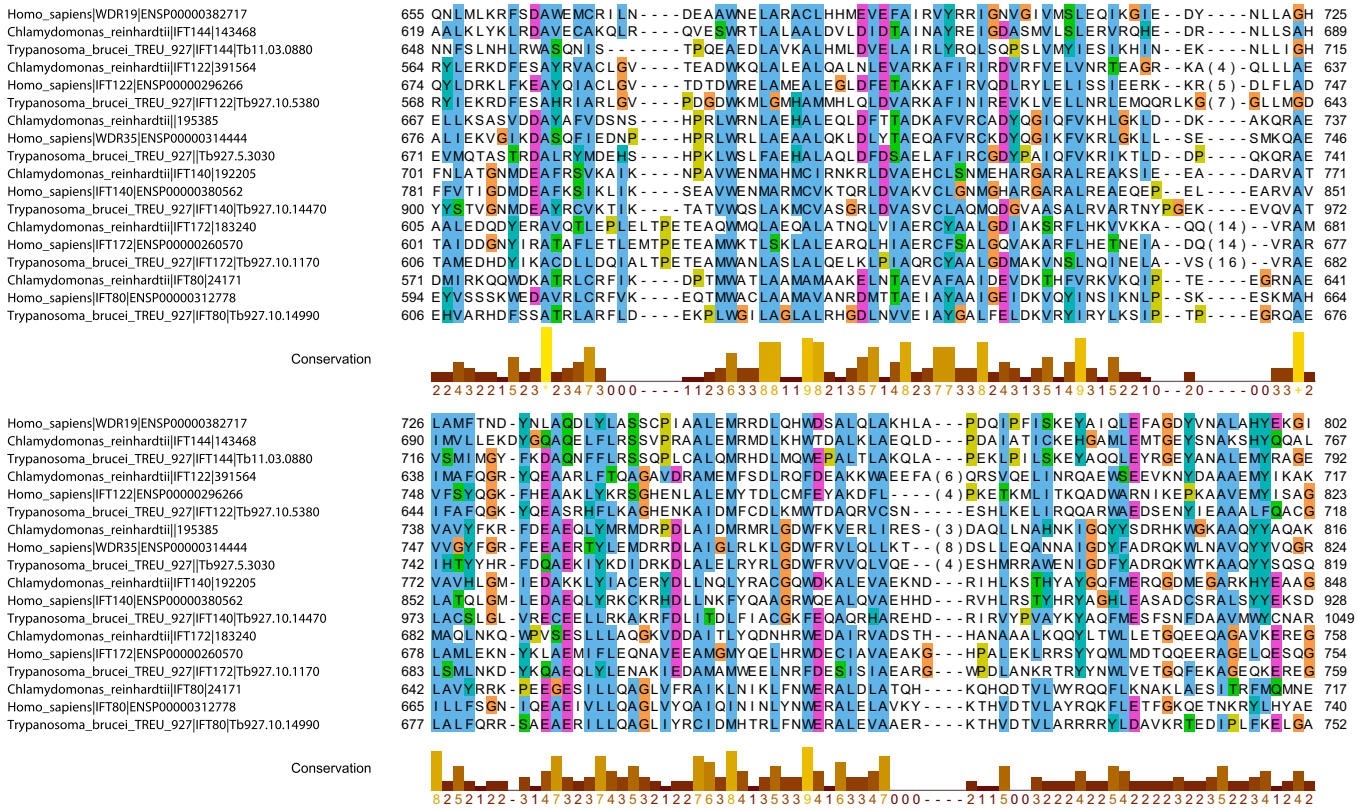

Fig. 2. Multiple sequence alignment of the αβ-IFT conserved region extracted from the full alignment. The full alignment contains 52 sequences. Larger inserts have been removed and are represented by number of residues removed between parentheses. An overview of the whole alignment is shown in Fig. S1.

(fungi, seed plants, *Phaeodactylum tricornutum*, and *Cryptosporidium parvum*, respectively).

This pattern of BBSome loss thus appears to precede the loss of the cilium, and may indicate a reduced role for cilia in BBSome-negative lineages before the cilium is lost entirely. The existence of multiple species with functional flagella, but lacking the BBSome, suggests that the BBSome is a nonessential component of IFT. The "moderate" importance of the BBSome is reflected in the viable, albeit sometimes severe, phenotypes associated with Bardet–Biedl syndrome in humans (8).

Disrupting the expression of BBSome subunits has profound effects on the other IFT complexes. BBSome dysfunction results in instability and incorrect assembly of the IFT complex, resulting in dissociated IFT-A and IFT-B complexes (9). This suggests that there is functional interaction between the BBSome and IFT-A and B. However, from our analysis, it appears that the removal of the BBSome can be tolerated in some species, indicating that this functional interaction must be nonessential. It will be interesting to understand how species compensate for loss of the BBSome, and what evolutionary steps are required to facilitate that loss. Consequently, this may provide insights into possible treatments for patients with Bardet–Biedl syndrome.

Further, the secondary loss of individual subunits observed in each subcomplex indicates that there may be a tolerance within the system for subunit loss. The phylogenetic patterns are potentially correlated with severity of mutant phenotype or the inner structure of the IFT complexes. Indeed, the pattern appears to be nonrandom: subunits of the IFT-B subcomplex that suffer the most losses (IFT74, IFT27, IFT22, and IFT25) are part of the salt-stable core (10–15) ($P = 0.029$, Fisher exact test; Table S2). Nevertheless, we did not observe a correlation between the number of losses of a subunit and the severity of its phenotype as measured by the severity of cilia length reduction ($P = 0.34$, Fisher exact test for the IFT-B complex; Table S2). This suggests that the conservation of an IFT subunit may depend more upon the structure of the IFT complex rather than the severity of the phenotype alteration in the mutant. Further biochemical research into the structures and mechanisms of the IFT may provide an explanation for this counterintuitive observation.

Orthologous IFT and BBSome Subunits from *Trypanosoma brucei* and *H. sapiens* Are Generally Conserved in Sequence and Structure. The variability in protein length and domain composition between homologous IFT subunits requires us to determine to which extent protein structure is conserved between subunits, as well as for orthologous subunits between eukaryotic species. We compared the sequences of the IFT and BBsome subunits in *T. brucei* and *H. sapiens* as well as their various predicted structural features, including secondary structure segments, disordered regions, coiled-coil regions, TPR repeats, and folds (Fig. 4 and Fig. S2). The orthologous IFT and BBSome subunit sequences are well conserved, despite the large evolutionary distances between them, and despite the variable presence of the subunits per species. For example, human IFT172 (1,749 residues) and *T. brucei* IFT172 (1,747 residues) have sequence identity of 41%, even though *T. brucei* belongs to the Excavata, an arguably early branching supergroup of eukaryotes (16, 17). The high similarity between the predicted secondary structure elements suggests that the orthologous proteins in the IFT complex are structurally conserved to a remarkable level.

We further explored structural similarities by comparing predicted coiled coils, disordered regions, TPR repeats, and fold types. Such an approach was instrumental in proposing a common ancestral protocoatomer for coated vesicle and nuclear pore subcomplexes, despite weak sequence similarities among the constituent subunits (2, 18). As for the sequences and secondary

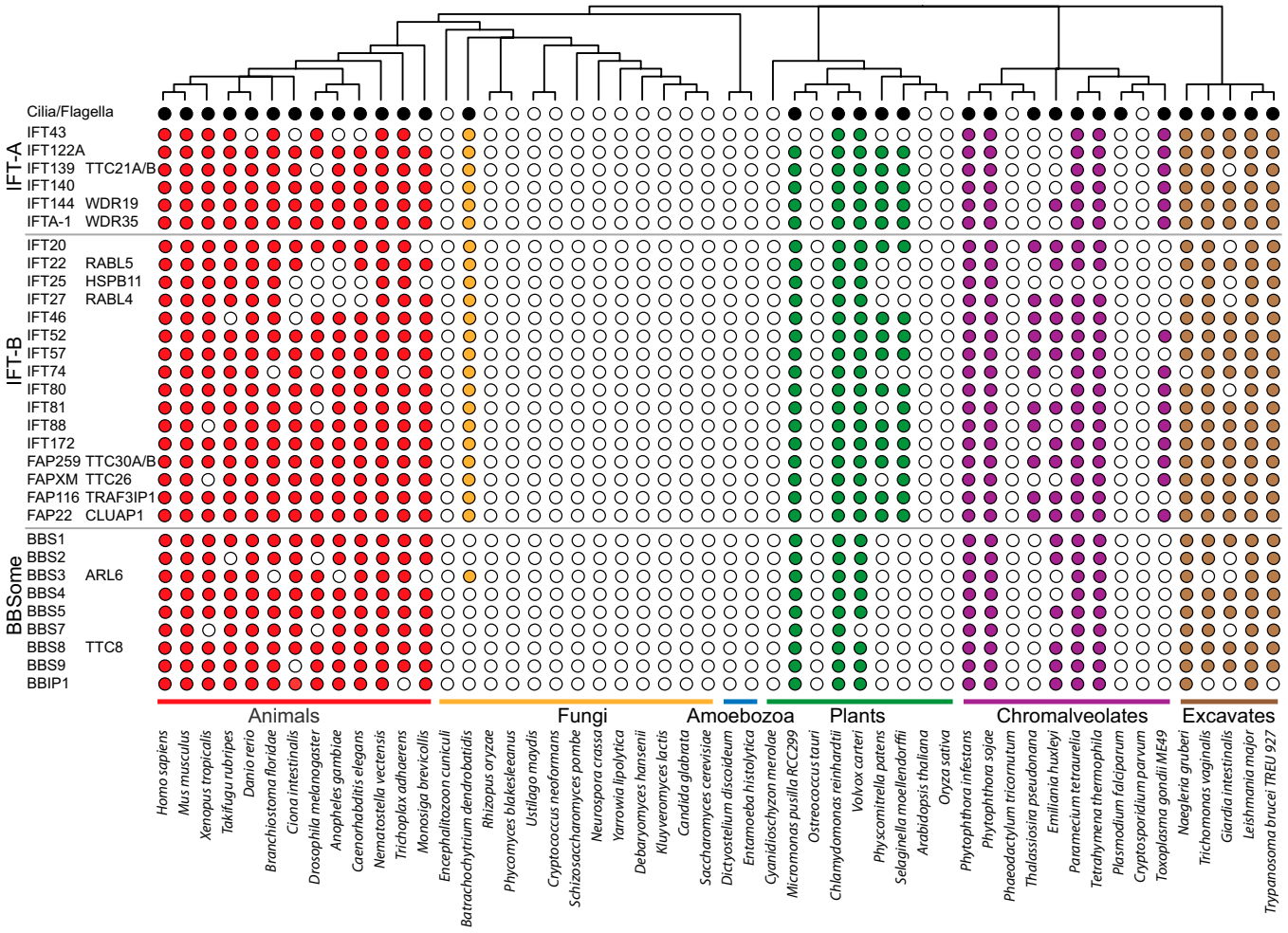

Fig. 3. Coulson plot demonstrating presence and absence (or loss) of IFT subunits in 52 eukaryotic genomes. Complexes are divided into IFT-A and -B and BBSome (rows), and taxa are displayed as columns. Super groups are color-coded for clarity, and phylogenetic relationships are shown at the top schematically. The presence of a cilium is also shown in the top row (black).

structure segments, the fold types are also conserved between orthologues from human and *T. brucei*. Moreover, fold types are likewise conserved among subunits within each of the three subcomplexes. Thus, the IFT and BBSome subunits can be organized into three structural classes as follows (Fig. 4). First, the ε-IFT subunits are all-α proteins with α-solenoid–like/TPR repeats, some of which contain disordered and/or coiled-coil regions (e.g., IFT88). Second, the αβ-IFT subunits consist of at least one β-propeller fold, followed by an α-helical region that may contain TPR repeats (e.g., WDR35). The exception is IFT80, which is predicted to contain only a short α-helical region unlikely to be a TPR repeat. The helical C terminus of the *T. brucei* IFT80 is longer than that of *H. sapiens*, perhaps indicating a significant structural difference within this one orthologous pair. Third, the BBSome subunits contain a β-propeller fold, followed by a short coiled-coil region and a C terminus that is rich in β-strands and α-helices. The folds of the C-terminal β-strand and α-helix–rich regions cannot be assigned reliably, although the α-helix–rich region in BBS9/PTHB1 exhibits distant sequence similarity to tropomyosin (Fig. S2).

Discussion

Our findings on the origin of the IFT subcomplexes and their subsequent loss in various lineages have implications for IFT evolution and structure. The phylogenetic reconstruction of the origins of the IFT subunits and observed modularity in the presence/absence profiles indicates that gain and loss of IFT components most likely occurred in distinct modular steps (Fig. 5). With respect to origins and acquisition of the IFT system, our results suggest that the BBSome and IFT-A emerged from an IFT-B–like complex by intracomplex duplications. Whether the IFT-A or the BBSome was the first additional subcomplex to emerge is unresolved at this time.

With respect to subsequent secondary losses, the apparent modularity of the IFT subcomplexes implies a distinct order to the loss of these factors, which, in some lineages, progressed to the loss of the cilium. We identified at least four independent loss events for the BBSome in *B. dendrobatidis*, *P. patens*, *S. moellendorffii*, *T. gondii* and *T. pseudonana*. All these taxa are closely related to species that have lost the cilium and IFT genes altogether (fungi, spermatophytes, *C. parvum*, and *P. tricornutum*, respectively; Fig. 3). Additionally, *T. pseudonana* has lost the IFT-A subcomplex. These observations suggest that the BBSome may be dispensed with while maintaining a level of cilium function. Subsequently the IFT-A subcomplex can be lost (*T. pseudonana*) before complete loss of IFT (*Plasmodium falciparum*) and of the cilium (*C. parvum*). These observations indicate that IFT-B could be viewed as the most critical subcomplex, as it is the last to be retained, and hence its presence essentially dictates if a cilium is present (Fig. 5). Stepwise emergence and loss suggests that IFT is an example of a "last-in,

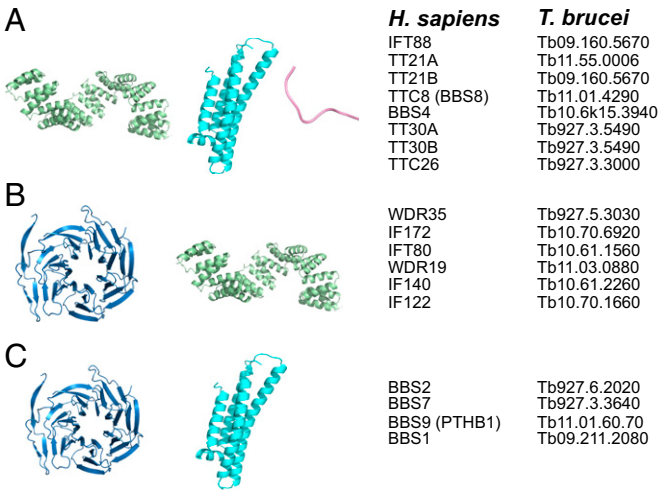

Fig. 4. Predicted fold types present within the IFT and BBSome subunits in *H. sapiens* and *T. brucei*. (*A*) ε-IFT subunits (yellow in Fig. 1*A*), (*B*) αβ-IFT subunits (blue in Fig. 1*A*), and (*C*) BBSome subunits (green in Fig 1*A*). The β-propeller fold is indicated in blue, the TPR/α-solenoid-like fold in green, a disordered region in pink, and a coiled coil in cyan.

first-out" evolutionary system, i.e., whereby modules added last are also the first ones to be lost.

A protocoatomer origin for IFT provides a rationale for involvement of IFT subunits in coated vesicle transport to the ciliary base (19). Subunits of the IFT and BBSome are implicated in various transport pathways, and, therefore, with respect to function, IFT has not fallen far from the coatomer tree. Whether IFT can function as a separate coatomer-like structure and whether individual IFT subunits associate with other coatomer complexes remains to be resolved; significantly, the BBSome has been suggested to function as a coatomer complex, as it has been shown to localize on to membranes and to assemble an electron dense coat (20).

The phylogenies of homologous IFT subunits provide a framework for elucidating IFT subunit assembly within the cilium. Mimicking the coatomer complexes, the αβ- and ε-IFT subunits likely have structural roles in IFT. By analogy to their homologous COPI subunits, they are likely to bind in a head-to-head and tail-to-tail configuration. Close paralogs could be expected to bind each other directly or to produce module variants by mutually exclusive binding with identical partners (21). The phylogenies therefore may assist by constraining the number of potential subunit arrangements. Although module variants remain to be described for IFT, there is a possibility that recently duplicated IFT subunits, such as TTC30A, TTC30B, TTC21A, and TTC21B, interact with the IFT in a mutually exclusive manner, further diversifying IFT function.

In conclusion, our results formally unite IFT with the coatomer protein complexes and the NPC, folding them into the protocoatomer family, as well as demonstrating that IFT is closely related to the COP I complex. Our phylogenetic reconstruction provides compelling evidence for functional as well as structural modularity within the IFT complex. Furthermore, the complex evolution of the IFT and its origin from a protocoatomer complex provides a keystone for understanding how the eukaryotic cell was able, by repurposing existing pathways and complexes, to evolve such a complex and highly organized organelle as the cilium.

Methods

Sequence Searches and Phylogenetic Analysis. We gathered protein sequences of 52 genomes of ciliated and nonciliated eukaryotes (Table S3). Orthologous IFT subunits were identified by OrthoMCL (version 2.0), followed by manual refinement based in part on HMMER (22) and PSI-BLAST (23) searches to find additional orthologues. Absences of subunits were checked against the respective genome with TBLASTN and available EST databases. The orthologous sequences were pruned to a limited set of diverse species to exclude problematic sequences but retain a wide phylogenetic coverage. Initial alignments were made with MAFFT LINSI (24). In the initial αβ′-like IFT subunit alignment, we observed a conserved region among all IFT subunits (*SI Discussion*). A custom HMM was made and was used to search against our 52 genomes. The final alignments were made by first aligning orthologous sequences for each IFT and COPI subunit and then progressively aligned with each other by OPAL (25) by using a neighbor-joining tree to guide the order of adding alignments. The neighbor-joining tree was constructed by using QuickTree (26) and the initial MAFFT-based alignment. The resulting alignments were then analyzed by using PhyML (27), RAxML (28), QuickTree, and PhyloBayes (29). The appropriate model of evolution (LG) was determined by PROTTEST (30). Proportion of invariable sites and

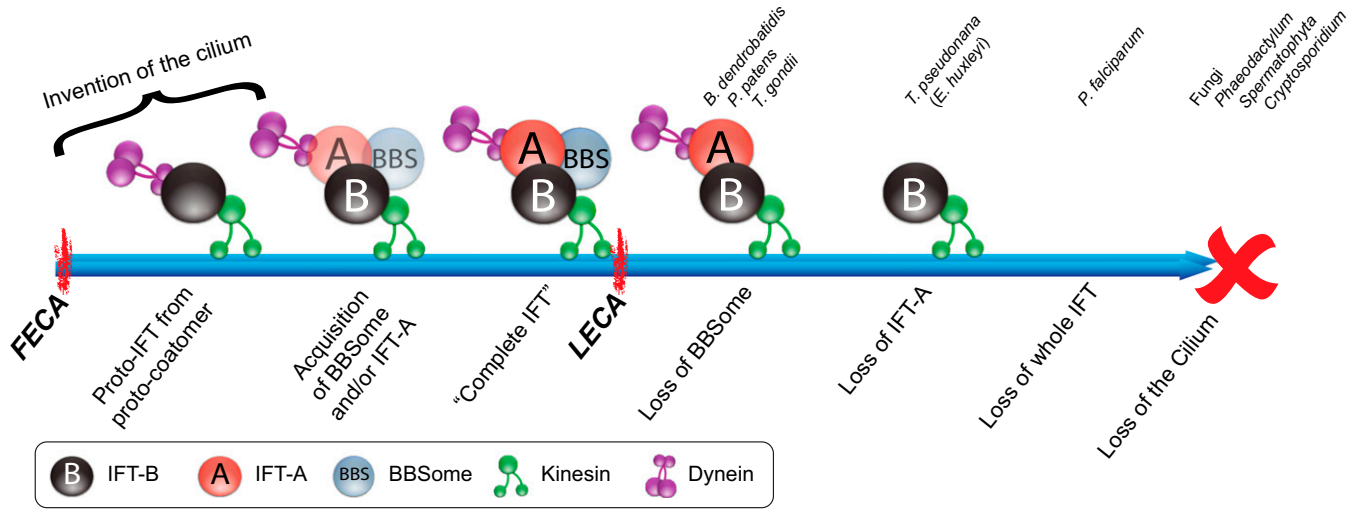

Fig. 5. Predicted origin and subsequent loss of each IFT subcomplex based on the phylogenetic trees for the COP-α–, COP-β′–, and COP-ε–like IFT subunits, as well as the presence/absence profiles of individual subunits. As a result of the absence of BBSome subunits in the αβ-like IFT phylogenetic tree, it is uncertain whether IFT-A or BBSome emerged as the second IFT subcomplex. The last common eukaryotic ancestor (LECA) already contained the complete set of IFT subunits observed in *C. reinhardtii*, *Leishmania major*, and humans, and this must have evolved in the transition between the last common eukaryotic ancestor and the first common eukaryotic ancestor (FECA). Species related to nonciliated species have lost the BBSome and, in one case, have also lost IFT-A.

γ-distribution shape parameters were estimated. The alternative topologies for the αβ′-like IFT subunits were created manually, and branch lengths were recalculated by using RAxML. Site log-likelihoods were calculated by using RAxML. Consel (31) was used to calculate the probabilities as shown in Table S4. Sequence similarity between the IFT and COP-ε subunits was detected by using HHsearch (32). Custom HMM models were constructed by using HMMER (v2). HMM models of the Panther database (5) were used as background to which the custom HMM models were compared.

Structure Analysis. IFT sequences were analyzed by using sequence-based methods for predicting disordered regions [IUPred; with default parameters (33)], coiled coils [MARCOIL; at threshold 90% (34)], and secondary structure elements [PSIPRED; with five PSI-BLAST iterations (35)]. In addition, the folds of full-length IFT sequences and their domains were predicted by the fold recognition servers pDomTHREADER/mGenTHREADER (36) and Phyre (37) (using the default parameters), as well as the comparative modeling server ModWeb (http://salilab.org/modweb; template selection performed by using sequence-sequence, sequence-profile, and profile-profile methods, with an E-value threshold of 1.0) (38) and TPRpred, a profile-sequence comparison tool trained for TPR repeats (39). Based on an initial inspection of the disorder, secondary structure, and fold predictions for full-length sequences, we estimated the domain boundaries for select sequences and resubmitted domain sequences to the fold assignment servers. High confidence fold predictions [Phyre (estimated precision ≥75%); pDomTHREADER (certainty of certain or score ≥6.2); MODWEB (Z-DOPE <0 or sequence identity ≥30%)] from individual servers were confirmed with the Pfam database entries. The final folds were assigned if more than one server predicted the same fold for a particular domain.

ACKNOWLEDGMENTS. We thank Isabel Duarte for comments on the phylogenetic analysis, Mike Rout for discussions on the evolution of the nuclear pore complex and related systems, and the research groups of Roepman and Kremer for valuable input on IFT function. This study was supported by the European Community's Seventh Framework Programme FP7/2009 under Grant 241955, SYSCILIA, Wellcome Trust Grant 082813 (to M.C.F.), and National Institutes of Health/National Institute of General Medical Sciences Grant U54 RR022220 (to A.S.).

1. Duldulao NA, Li J, Sun Z (2010) Cilia in cell signaling and human disorders. *Protein Cell* 1:726–736.
2. Devos D, et al. (2004) Components of coated vesicles and nuclear pore complexes share a common molecular architecture. *PLoS Biol* 2(12):e380.
3. Avidor-Reiss T, et al. (2004) Decoding cilia function: Defining specialized genes required for compartmentalized cilia biogenesis. *Cell* 117(4):527–539.
4. Jékely G, Arendt D (2006) Evolution of intraflagellar transport from coated vesicles and autogenous origin of the eukaryotic cilium. *Bioessays* 28(2):191–198.
5. Thomas PD, et al. (2003) PANTHER: A browsable database of gene products organized by biological function, using curated protein family and subfamily classification. *Nucleic Acids Res* 31(1):334–341.
6. Hodges ME, Wickstead B, Gull K, Langdale JA (2012) The evolution of land plant cilia. *New Phytol* 195(3):526–540.
7. Briggs LJ, Davidge JA, Wickstead B, Ginger ML, Gull K (2004) More than one way to build a flagellum: Comparative genomics of parasitic protozoa. *Curr Biol* 14(15): R611–R612.
8. Forsythe E, Beales PL (2013) Bardet-Biedl syndrome. *Eur J Hum Genet* 21:8–13.
9. Wei Q, et al. (2012) The BBSome controls IFT assembly and turnaround in cilia. *Nat Cell Biol* 14(9):950–957.
10. Lucker BF, Miller MS, Dziedzic SA, Blackmarr PT, Cole DG (2010) Direct interactions of intraflagellar transport complex B proteins IFT88, IFT52, and IFT46. *J Biol Chem* 285(28):21508–21518.
11. Taschner M, Bhogaraju S, Lorentzen E (2012) Architecture and function of IFT complex proteins in ciliogenesis. *Differentiation* 83(2):S12–S22.
12. Wang Z, Fan Z-C, Williamson SM, Qin H (2009) Intraflagellar transport (IFT) protein IFT25 is a phosphoprotein component of IFT complex B and physically interacts with IFT27 in Chlamydomonas. *PLoS ONE* 4(5):e5384.
13. Bhogaraju S, Taschner M, Morawetz M, Basquin C, Lorentzen E (2011) Crystal structure of the intraflagellar transport complex 25/27. *EMBO J* 30(10):1907–1918.
14. Fan Z-C, et al. (2010) Chlamydomonas IFT70/CrDYF-1 is a core component of IFT particle complex B and is required for flagellar assembly. *Mol Biol Cell* 21(15):2696–2706.
15. Richey EA, Qin H (2012) Dissecting the sequential assembly and localization of intraflagellar transport particle complex B in Chlamydomonas. *PLoS ONE* 7(8):e43118.
16. Simpson AGB, Roger AJ (2004) The real 'kingdoms' of eukaryotes. *Curr Biol* 14(17): R693–R696.
17. Roger AJ, Simpson AGB (2009) Evolution: Revisiting the root of the eukaryote tree. *Curr Biol* 19(4):R165–R167.
18. Devos D, et al. (2006) Simple fold composition and modular architecture of the nuclear pore complex. *Proc Natl Acad Sci USA* 103(7):2172–2177.
19. Baldari CT, Rosenbaum J (2010) Intraflagellar transport: It's not just for cilia anymore. *Curr Opin Cell Biol* 22(1):75–80.
20. Jin H, et al. (2010) The conserved Bardet-Biedl syndrome proteins assemble a coat that traffics membrane proteins to cilia. *Cell* 141(7):1208–1219.
21. Szklarczyk R, Huynen MA, Snel B (2008) Complex fate of paralogs. *BMC Evol Biol* 8:337.
22. Eddy SR (1998) Profile hidden Markov models. *Bioinformatics* 14(9):755–763.
23. Altschul SF, et al. (1997) Gapped BLAST and PSI-BLAST: A new generation of protein database search programs. *Nucleic Acids Res* 25(17):3389–3402.
24. Katoh K, Misawa K, Kuma K, Miyata T (2002) MAFFT: A novel method for rapid multiple sequence alignment based on fast Fourier transform. *Nucleic Acids Res* 30(14):3059–3066.
25. Wheeler TJ, Kececioglu JD (2007) Multiple alignment by aligning alignments. *Bioinformatics* 23(13):i559–i568.
26. Howe K, Bateman A, Durbin R (2002) QuickTree: Building huge Neighbour-Joining trees of protein sequences. *Bioinformatics* 18(11):1546–1547.
27. Guindon S, Gascuel O (2003) A simple, fast, and accurate algorithm to estimate large phylogenies by maximum likelihood. *Syst Biol* 52(5):696–704.
28. Stamatakis A, Ludwig T, Meier H (2005) RAxML-III: A fast program for maximum likelihood-based inference of large phylogenetic trees. *Bioinformatics* 21(4):456–463.
29. Lartillot N, Lepage T, Blanquart S (2009) PhyloBayes 3: A Bayesian software package for phylogenetic reconstruction and molecular dating. *Bioinformatics* 25(17):2286–2288.
30. Darriba D, Taboada GL, Doallo R, Posada D (2011) ProtTest 3: Fast selection of best-fit models of protein evolution. *Bioinformatics* 27(8):1164–1165.
31. Shimodaira H, Hasegawa M (2001) CONSEL: For assessing the confidence of phylogenetic tree selection. *Bioinformatics* 17(12):1246–1247.
32. Söding J (2005) Protein homology detection by HMM-HMM comparison. *Bioinformatics* 21(7):951–960.
33. Dosztányi Z, Csizmok V, Tompa P, Simon I (2005) IUPred: Web server for the prediction of intrinsically unstructured regions of proteins based on estimated energy content. *Bioinformatics* 21(16):3433–3434.
34. Delorenzi M, Speed T (2002) An HMM model for coiled-coil domains and a comparison with PSSM-based predictions. *Bioinformatics* 18(4):617–625.
35. McGuffin LJ, Bryson K, Jones DT (2000) The PSIPRED protein structure prediction server. *Bioinformatics* 16(4):404–405.
36. Lobley A, Sadowski MI, Jones DT (2009) pGenTHREADER and pDomTHREADER: New methods for improved protein fold recognition and superfamily discrimination. *Bioinformatics* 25(14):1761–1767.
37. Kelley LA, Sternberg MJE (2009) Protein structure prediction on the Web: A case study using the Phyre server. *Nat Protoc* 4(3):363–371.
38. Pieper U, et al. (2009) MODBASE, a database of annotated comparative protein structure models and associated resources. *Nucleic Acids Res* 37(database issue): D347–D354.
39. Karpenahalli MR, Lupas AN, Söding J (2007) TPRpred: A tool for prediction of TPR-, PPR- and SEL1-like repeats from protein sequences. *BMC Bioinformatics* 8:2.

Supporting Information

van Dam et al. 10.1073/pnas.1221011110

SI Discussion

Common Descent of Intraflagellar Transport and Coat Protein Complex I-α and -β′ Subunits. We constructed phylogenetic trees for the βα–intraflagellar transport (IFT) subunits, coat protein complex (COP)-α and COP-β′ (Fig. S3*A*). The tree topology (Fig. S3*A*) is representative of trees constructed by using maximum-likelihood and neighbor-joining methods. The IFT-B and IFT-A complex subunits (IFT80, IFT172 and IFT140, IFT122, WDR35, and WDR19, respectively) are resolved between two branches. However, the support at node *d* is low (49, 49, and 67 for RAxML, PhyML and QuickTree, respectively) and indicates that alternative topologies are possible, and placement of this node is ambiguous (Fig. S3 *B* and *C*). Bayesian phylogenetic methods reported, at best, a trifurcation for the IFT80, IFT172, and IFT-A subunits. We performed topology testing as implemented in Consel (1) (Table S4). None of the three topologies can be rejected at approximately unbiased test $P > 0.05$. Therefore, we cannot select a definitive phylogenetic reconstruction from among these three possibilities.

Our phylogenetic analysis of the βα-IFT, COP-α, and COP-β′ subunits suggests at least two possible evolutionary scenarios. In one scenario, IFT-A– and IFT-B–specific subunits emerged concurrently by the duplication of a single βα-IFT subunit, followed by subsequent specializations (Fig. S3*D*). In the second scenario, the ancestral βα-IFT subunit initially gave rise to IFT-B subunits, and IFT-A subunits emerged later (Fig. S3*E*). The latter scenario suggests that the earliest IFT complex was IFT-B–like, similar to that found for ε-IFT.

BBSome and Protocoatomer Origin. Jin et al. showed that the BBSome assembles as part of a vesicle coat to traffic proteins to the base of the cilium (2). Their predictions of the structure of BBS subunits indicate that the BBSome exhibits a combination of protein structures that is typical of a coatomer like structure, e.g., β-propeller and α-solenoid structures (Fig. 4 and Fig. S2), and that BBS1, -2, -7, and -9 (green in Fig. 1*A*) have the predicted protein structures of a β-propeller (Fig. 3 and Fig. S2). However, the α-solenoid structure is confined to the BBS4 and BBS8 subunits, which we show to be homologous to COP-ε and IFT-A and -B complex subunits IFT88, TTC26, TTC30A and B, and TTC21.

By using sensitive homology searches, we found evidence that BBS1, 2, 7, and 9 are directly related to each other (Table S5). However, we did not find any sequence similarity outside of the BBSome and therefore are unable to link the origin of these BBSome subunits to the protocoatomer complexes or other IFT subunits. The origin of BBS4 and BBS8 from an ancestral ε-IFT subunit argues against an independent origin of the BBSome and IFT as coatomer-like complexes, and argues instead for convergent evolution of the structures of the BBS1, -2, -7, and -9 subunits to resemble the coatomer β-propeller structure.

Independent Acquisitions of Small GTPases into IFT. BBS3 (ARL6), IFT22 (RabL5), and IFT27 (RabL4) belong to the Ras-like superfamily of small GTPases (Fig. 1*C*, red). BBS3 is an Arf-like GTPase, a subfamily of small GTPases that includes ARF1, a subunit of COPI. The IFT22 GTPase is most interesting as this GTPase cannot be assigned to any of the classical GTPase subfamilies, e.g., Arf, Rab, Ras, or Rho (3). IFT27 is a Rab-like GTPase, and, although phylogenetic evidence is conflicting (3, 4), this is supported by the presence of Rab-specific sequence motifs. Although not discussed in these articles, the published phylogenetic analyses on the small GTPase superfamily indicates that BBS3, IFT27, and IFT22 were recruited to the IFT complex independently, as they are not each other's closest paralogs.

The presence of three small GTPases, known for their regulatory functions, mark an apparent high level of regulation required for effective IFT. Independent recruitment of several small GTPases indicates that this regulation was likely acquired in a stepwise manner as IFT complexity grew in size.

Cilium and Flagellar Structure and Function in Species with Degenerate IFT. Differential loss of IFT subunits begs the question of how cilia function in those species with a reduced IFT system. *Batrachochytrium dendrobatidis* is an important species in this context as it represents the chytrid fungi, the only fungal group with functional and motile flagella. The *B. dendrobatidis* flagellum has a normal 9+2 axoneme (5), but lacks the BBSome. Interestingly BBS3, an Arf-like small GTPase, is retained, suggesting an additional role for BBS3 outside of the BBSome (Fig. 3).

Selaginella moellendorffii (lycophyte) and *Physcomitrella patens* (moss) represent early-branching species of vascular land plants. *S. moellendorffii* and *P. patens* pollen have motile cilia that aid in successful fertilization by chemotaxis (6). Most species of spermatophytes (i.e., seed plants), on the contrary, have lost cilia completely, with the exception of Cycads and Gingko plants (7). *S. moellendorffii* and *P. patens* lack the BBSome, but, significantly, *P. patens* cilia are reported to have a normal basal body and 9+2 axoneme structure (5), similar to *B. dendrobatidis*.

Toxoplasma gondii is a protozoan parasite belonging to the Apicomplexa and is a relative of *Plasmodium falciparum* and *Cryptosporidium parvum*. *T. gondii* and *P. falciparum* microgametes are flagellated (8, 9), whereas *C. parvum* is not (10). The Apicomplexa species underwent a number of significant modifications to their flagellar machinery and therefore represent evolutionary "snapshots" in which the flagellum was apparently lost in stages. Briggs et al. showed that *T. gondii* has IFT subunits but lacks the BBSome (11) (Fig. 5). *P. falciparum* has lost all IFT subunits but still constructs motile flagella in the microgamete stage, but the flagellar axoneme is constructed in the cytosol, probably circumventing a need for IFT (9). Finally, *C. parvum* has lost the IFT and does not construct flagella at any point in the known life cycle (10).

Thalassiosira pseudonana [9+0 axoneme, with normal basal body architecture (5)] appears to have lost both the BBSome and the IFT-A complex. How closely the *T. pseudonana* flagellum resembles the well known flagellar phenotype in, for instance, *Chlamydomonas reinhardtii* is unknown. However, the presence of cilium genes indicates that *T. pseudonana* is able to maintain some sort of flagellar structure, and with only an IFT-B complex. The structure and functionality of the *T. pseudonana* flagellum would be of value here as it may provide a model for a minimal, but functional, IFT.

T. gondii, *P. falciparum*, and *T. pseudonana* are ciliated species that not only share the lack of the BBSome, they also share a common mechanism for alternative motility. Diatoms and Apicomplexa have an actin-myosin–based mechanism that enables them to glide through viscous substrates (12, 13). This alternative mechanism for motility could be an explanation for the degenerate state of the IFT as the cilium apparently is no longer essential for movement.

1. Shimodaira H, Hasegawa M (2001) CONSEL: For assessing the confidence of phylogenetic tree selection. *Bioinformatics* 17(12):1246–1247.
2. Jin H, et al. (2010) The conserved Bardet-Biedl syndrome proteins assemble a coat that traffics membrane proteins to cilia. *Cell* 141(7):1208–1219.
3. Rojas AM, Fuentes G, Rausell A, Valencia A (2012) The Ras protein superfamily: Evolutionary tree and role of conserved amino acids. *J Cell Biol* 196(2):189–201.
4. Elias M, Brighouse A, Gabernet-Castello C, Field MC, Dacks JB (2012) Sculpting the endomembrane system in deep time: High resolution phylogenetics of Rab GTPases. *J Cell Sci* 125(pt 10):2500–2508.
5. Carvalho-Santos Z, et al. (2010) Stepwise evolution of the centriole-assembly pathway. *J Cell Sci* 123(pt 9):1414–1426.
6. Maier I (1993) Gamete orientation and induction of gametogenesis by pheromones in algae and plants. *Plant Cell Environ* 16:891–907.
7. Renzaglia KS, Garbary DJ (2001) Motile gametes of land plants: Diversity, development, and evolution. *Crc Cr Rev Plant Sci* 20:107–213.
8. Ferguson DJ (2002) Toxoplasma gondii and sex: Essential or optional extra? *Trends Parasitol* 18(8):351–355.
9. Sinden RE, Talman A, Marques SR, Wass MN, Sternberg MJ (2010) The flagellum in malarial parasites. *Curr Opin Microbiol* 13(4):491–500.
10. Mehlhorn H, ed. (2001) Cryptosporidium species. *Encyclopedic Reference of Parasitology* (Springer, Heidelberg), pp 143–144.
11. Briggs LJ, Davidge JA, Wickstead B, Ginger ML, Gull K (2004) More than one way to build a flagellum: Comparative genomics of parasitic protozoa. *Curr Biol* 14(15): R611–R612.
12. Poulsen NC, Spector I, Spurck TP, Schultz TF, Wetherbee R (1999) Diatom gliding is the result of an actin-myosin motility system. *Cell Motil Cytoskeleton* 44(1):23–33.
13. Sibley LD, Håkansson S, Carruthers VB (1998) Gliding motility: An efficient mechanism for cell penetration. *Curr Biol* 8(1):R12–R14.

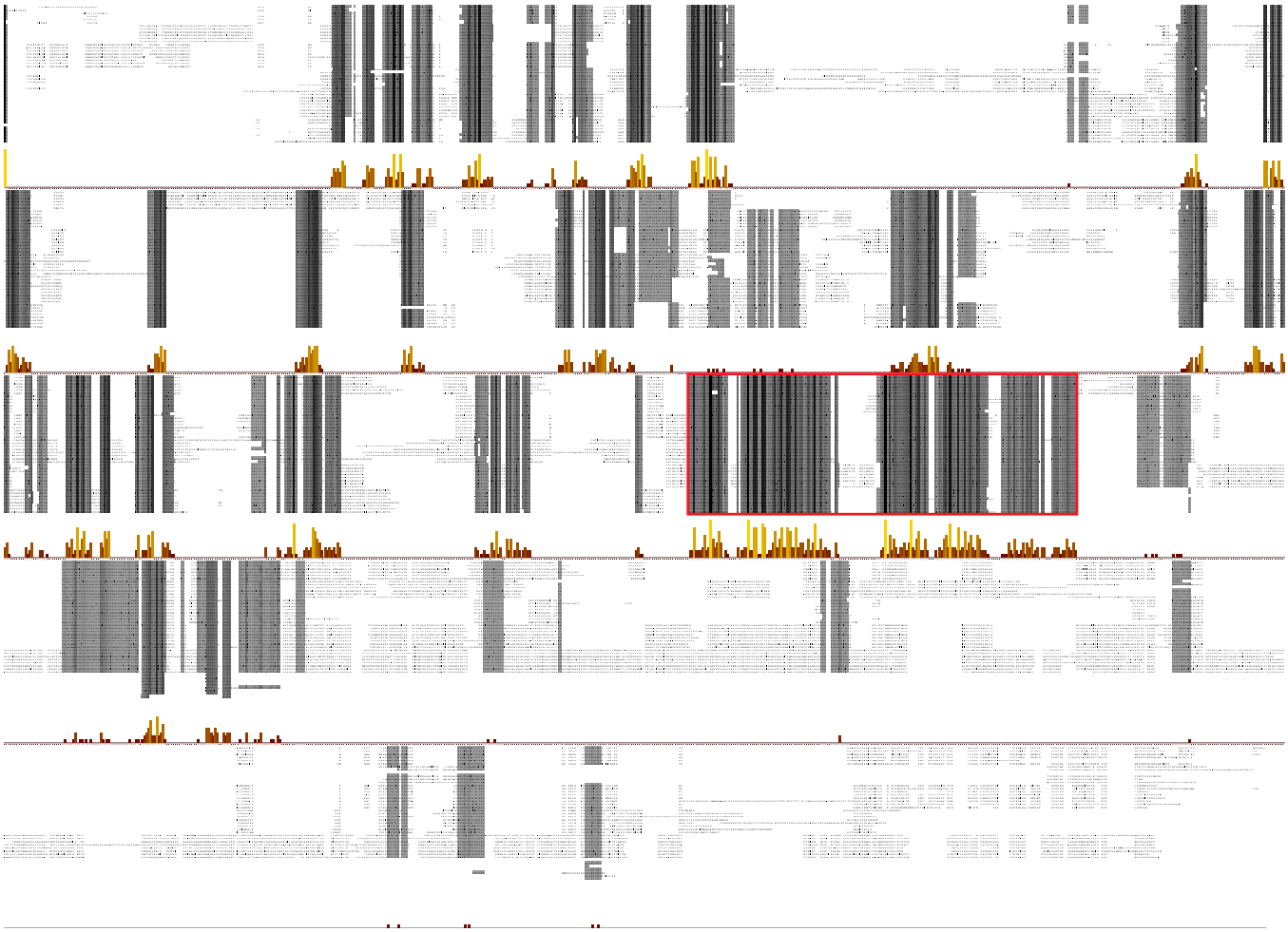

Fig. S1. Full alignment of the αβ-IFT subunits. The background coloring indicates conservation, with black being the most conserved. A section of ∼150 residues (red rectangle; Fig. 2) was used to create a hidden Markov model.

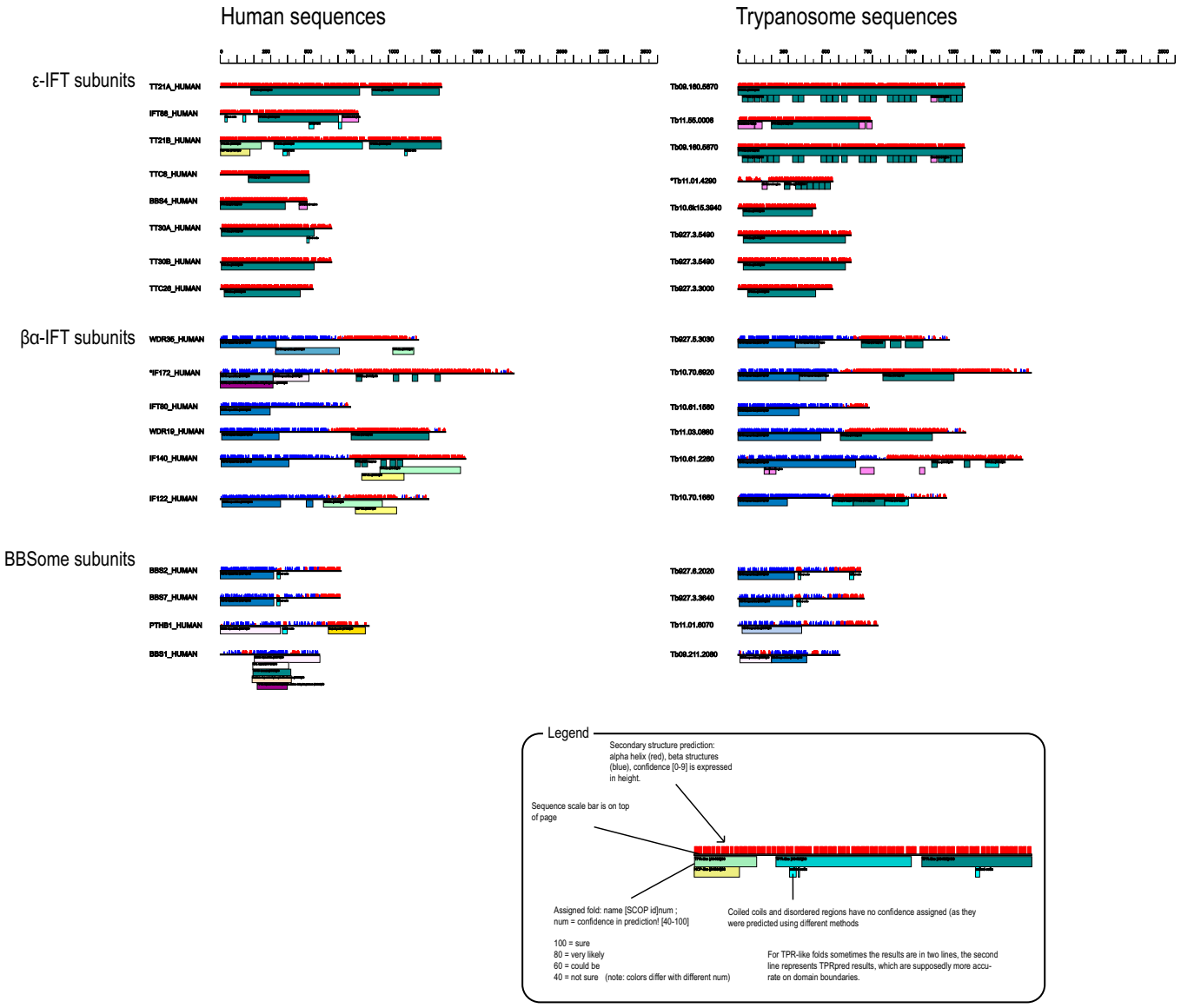

Fig. S2. Predicted structures for the human and trypanosome IFT and BBSome subunits. The predicted secondary structure and fold as well as disordered and coiled-coil regions are visualized for each subunit sequence of the three complexes in human (*Left*) and trypanosome (*Right*) as indicated. *Methods* provides prediction protocols.

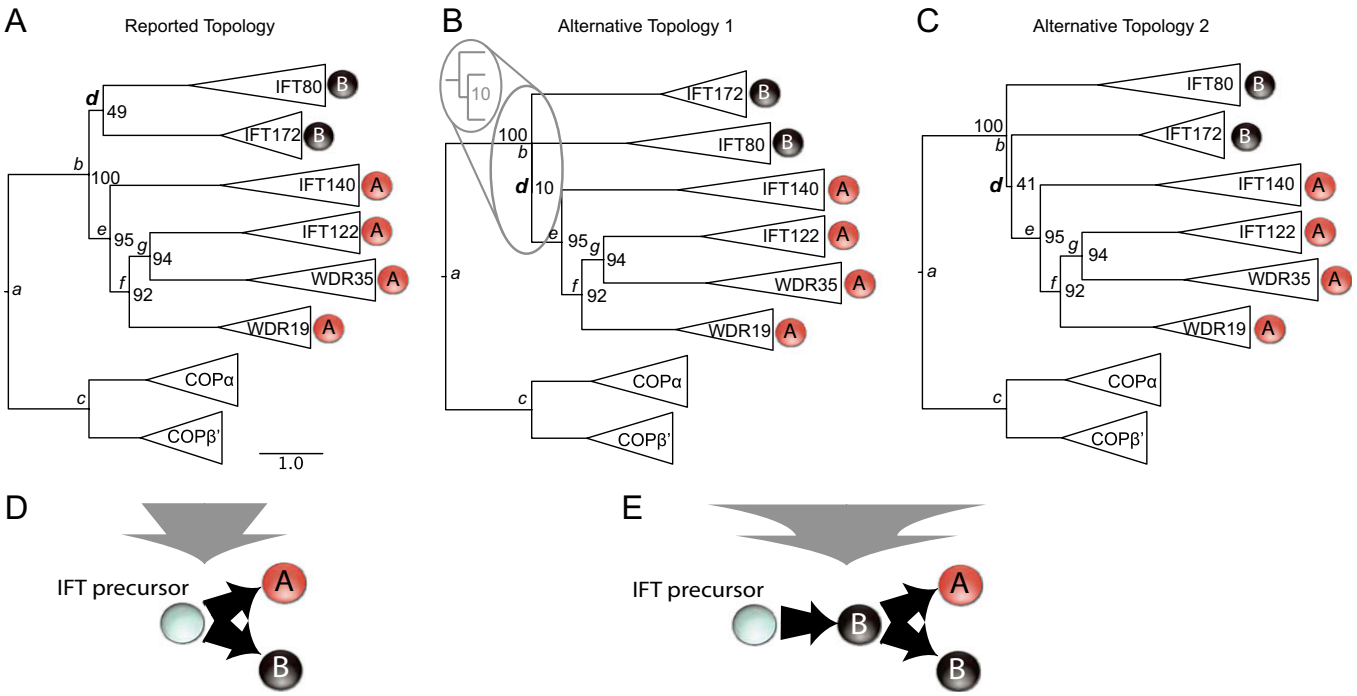

Fig. S3. Phylogenetic analyses of the βα-IFT and ε-IFT subunits. (*A*) The reported tree for βα-IFT by RAxML, also representative for maximum-likelihood and neighbor-joining methods, indicates an unsupported bifurcation at node *d*. Alternative topologies (*B* and *C*) are depicted with bootstrap values for node *d* in bold. (*D* and *E*) Derived evolutionary scenarios for the origin of IFT-A and IFT-B subcomplexes based on the βα-IFT trees depicted above.

Table S1. HMM-HMM comparisons of ε-IFT and COP-ε using HHPred

Query/hit	BBS4	BBS8	TTC21	IFT88	TTC26	TTC30	COPE
BBS4	0	2.8×10^{-45}	2.6×10^{-26}	1.2×10^{-21}	6.2×10^{-14}*	1.4×10^{-12}*	9×10^{-11}*
BBS8	3.8×10^{-44}	0	3.4×10^{-16}*	2.8×10^{-20}	1.2×10^{-7}*	5.9×10^{-10}*	4.4×10^{-8}*
TTC21	6.1×10^{-23}	1.5×10^{-14}	0	6.1×10^{-21}	5.9×10^{-12}	1.9×10^{-12}	3.8×10^{-8}
IFT88	3×10^{-19}	1.8×10^{-18}	2.7×10^{-21}	0	3.4×10^{-7}*	1.4×10^{-17}	3.8×10^{-5}*
TTC26	3.5×10^{-13}	2.3×10^{-7}	8×10^{-13}	3.8×10^{-7}	0	1.9×10^{-25}	2.3×10^{-6}
TTC30	6.2×10^{-11}	7.4×10^{-9}	3.2×10^{-12}	4.6×10^{-17}	4×10^{-23}	0	5.8×10^{-5}
COPE	7×10^{-11}	2.4×10^{-8}	3.2×10^{-9}	1×10^{-5}	8.3×10^{-7}	1.1×10^{-5}	0

COPE is overall the most significant non-IFT hit in database searches using the mentioned IFT subunits as query. HMM, hidden Markov model.

*HMM-HMM combinations intersected by higher-scoring Panther HMMs. These Panther HMMs were not consistently retrieved as high scoring for other IFT subunits.

Table S2. List of IFT components and number of losses as used for the calculations of the *P* values to determine the relationship between complex structure, phenotypes, and number of losses suffered by subunits

Subunit	Alternate name	No. of Losses	IFT-B salt stable core	Ciliogenesis defect	Reference PubMed ID
IFTA					
IFT43	—	11	—	Moderate defect	19450523
IFT122A	—	3	—	Moderate defect	19450523
IFT139	TTC21A/B	5	—	Moderate defect	19450523
IFT140	—	3	—	Moderate defect	19450523
IFT144	WDR19	2	—	Moderate defect	19450523
IFTA-1	WDR35	3	—	Moderate defect	19450523
IFTB					
IFT20	—	3	No	Strong defect	19450523
IFT22	RABL5	7	Yes	No defect	19450523
IFT25	HSPB11	15	Yes	No defect	22595669
IFT27	RABL4	9	Yes	Moderate defect	19450523
IFT46	—	4	Yes	Strong defect	19450523
IFT52	—	1	Yes	Strong defect	19450523
IFT57	—	2	No	Moderate defect	19450523
IFT74	—	8	Yes	Moderate defect	19450523
IFT80	—	4	No	Strong defect	19450523
IFT81	—	3	Yes	Moderate defect	19450523
IFT88	—	3	Yes	Strong defect	19450523
IFT172	—	2	No	Strong defect	19450523
FAP259	TTC30A/B	1	Yes (IFT70)	Moderate defect	19450523
FAPXM	TTC26	5	No	Strong defect	22718903
FAP116	TRAF3IP1	2	No	Strong defect	21945076
FAP22	CLUAP1	1	No	Strong defect	23351563

Fisher exact tests were based on the median of three losses as cutoff and "salt stable core" vs. "not-salt stable core" and "severe phenotype" vs. "moderate to no phenotype."

Table S3. List of genomes used in this study

Taxonomy ID	Name	Phylum	Description	Source	Assembly version	Date	
						File on server	Downloaded
9606	*Homo sapiens*	Primates	Human	EnsEMBL release 59	GRCh37	2009-02-01	2010-10-14
10090	*Mus musculus*	Rodentia	Mouse	EnsEMBL release 59	NCBIM37	2007-04-01	2010-10-14
8364	*Xenopus tropicalis*	Amphibia	Frog	EnsEMBL release 60	Joint Genome Institute 4.1	2005-08-01	2010-11-10
31033	*Takifugu rubripes*	Actinopterygii	Pufferfish	EnsEMBL release 59	4	2004-10-01	2010-10-13
7955	*Danio rerio*	Actinopterygii	Zebrafish	EnsEMBL release 59	Zv8	2008-06-12	2010-10-14
7739	*Branchiostoma floridae*	Cephalochordata	Lancetfish	Joint Genome Institute DOE	V1.0	2008-06-19	2010-10-14
7719	*Ciona intestinalis*	Urochordata	Sea squirt	EnsEMBL release 59	2	2002-10-01	2010-10-13
7227	*Drosophila melanogaster*	Brychycera	Fruitfly	EnsEMBL release 59	BDGP assembly release 5	2006-04-01	2010-10-14
7165	*Anopheles gambiae*	Nematocera	Mosquito	EnsEMBL Metazoa release 6	AgamP3	2006-02-01	2010-10-13
6239	*Caenorhabditis elegans*	Nematoda	Nematode worm	EnsEMBL release 59	Wormbase WS210	2010-01-01	2010-10-14
45351	*Nematostella vectensis*	Cnidaria	Sea anemone	Joint Genome Institute DOE	V1.0	—	2010-10-14
10228	*Trichoplax adhaerens*	Placozoa	Placozoan	Joint Genome Institute DOE	V1.0	2006-08-30	2010-10-14
81824	*Monosiga brevicollis*	Choanoflagellida	Choanoflagellate	Joint Genome Institute DOE	V1.0	2006-07-01	2010-10-14
6035	*Encephalitozoon cuniculi*	Microsporidia	Microsporidium	EMBL Integr8	NA	—	2010-10-14
109871	*B. dendrobatidis*	Chytridiomycota	Chytrid fungus	Joint Genome Institute DOE	V1.0	2008-03-04	2010-10-14
64495	*Rhizopus oryzae*	Zygomycota	Fungus	BROAD	—	2005-11-01	2010-10-14
4837	*Phycomyces blakesleeanus*	Zygomycota	Fungus	Joint Genome Institute DOE	V2.0	2010-03-01	2010-10-14
5270	*Ustilago maydis*	Basidiomycota	Fungus	BROAD	Release 2	2004-03-01	2010-10-14
5207	*Cryptococcus neoformans*	Basidiomycota	Fungus	BROAD	v4	2008-08-12	2010-10-14
5141	*Neurospora crassa*	Pezizomycotina	Filamentous fungus	BROAD	6/25/10	2010-06-25	2010-10-14
4896	*Schizosaccharomyces pombe*	Taphrinomycotina	Fission yeast	EnsEMBL Fungi release 6	GeneDB Spombe release 2007	2005-06-29	2010-10-14
4952	*Yarrowia lipolytica*	Dipodascaceae	Yeast	Genoscope	Release 3	2003-09-10	2010-10-14
4959	*Debaryomyces hansenii*	Saccharomycetaceae	Yeast	Genoscope	Release 2	2008-09-10	2010-10-14
28985	*Kluyveromyces lactis*	Saccharomycetaceae	Yeast	Genoscope	Release 3	2008-09-10	2010-10-14
5478	*Candida glabrata*	Saccharomycetaceae	Yeast	Genoscope	Release 3	2008-09-10	2010-10-14
4932	*Saccharomyces cerevisiae*	Saccharomycetaceae	Bakers yeast	EnsEMBL Fungi release 6	SGD Scerevisiae import March 2010	2010-03-01	2010-10-14
44689	*Dictyostelium discoideum*	Amoebozoa	Slime mold	Dictybase	—	2010-10-12	2010-10-14
5759	*Entamoeba histolytica*	Amoebozoa	Amoeba	Sanger	10/21/05	2005-10-21	2010-10-14
45157	*Cyanidioschyzon merolae*	Rhodophyta	Red algae	*Cyanidioschyzon merolae* Genome Project	7/10/07	2007-07-10	2010-10-14
296587	*Micromonas pusilla* RCC299	Chlorophyta	Green algae	Joint Genome Institute DOE	V2.0	2009-04-01	2010-10-14
70448	*Ostreococcus tauri*	Chlorophyta	Green algae	Joint Genome Institute DOE	V2.0	—	2010-10-14
3055	*C. reinhardtii*	Chlorophyta	Green algae	Joint Genome Institute DOE	V4.0	2009-03-04	2010-10-14
3067	*Volvox carteri*	Chlorophyta	Green algae	Joint Genome Institute DOE	V1.0	2007-03-01	2010-10-14
3218	*P. patens*	Bryophyta	Moss	Joint Genome Institute DOE	V1.1	2009-04-10	2010-10-14
88036	*S. moellendorffii*	Lycopodiophyta	Lycophyte	Joint Genome Institute DOE	V1.0	2007-12-20	2010-10-14
3702	*Arabidopsis thaliana*	Dicot	Thale cress	TAIR	—	2009-06-19	2010-10-14
4530	*Oryza sativa*	Monocot	Rice	PlantGDB	—	2010-05-07	2010-10-14
4787	*Phytophthora infestans*	Oomycetes	Water mold	BROAD	—	—	2010-10-14
67593	*Phytophthora sojae*	Oomycetes	Water mold	Joint Genome Institute DOE	V1.1	2004-08-01	2010-10-14
2850	*Phaeodactylum tricornutum*	Bacillariophyta	Diatome	Joint Genome Institute DOE	V2.0	2007-05-01	2010-10-14
35128	*T. pseudonana*	Bacillariophyta	Diatome	Joint Genome Institute DOE	v3.0	2007-05-01	2010-10-14
2903	*Emiliania huxleyi*	Haptophyta	Protozoan	Joint Genome Institute DOE	V1.0	2008-04-25	2010-10-14
5888	*Paramecium tetraurelia*	Ciliophora	Paramecium	ParameciumDB	V1.48	2010-10-06	2010-10-14

Table S3. Cont.

Taxonomy ID	Name	Phylum	Description	Source	Assembly version	Date	
						File on server	Downloaded
5911	*Tetrahymena thermophila*	Ciliophora	Tetrahymena	ciliate.org	—	2004-08-01	2010-10-14
5833	*P. falciparum*	Apicomplexa	Protozoan	PlasmoDB	V7.0	2010-09-12	2010-10-14
5807	*C. parvum*	Apicomplexa	Protozoan	CryptoDB	V4.3	2010-09-13	2010-10-14
508771	*T. gondii* ME49	Apicomplexa	Protozoan	ToxoDB v6.2	7/16/08	2010-09-13	2010-10-14
5762	*Naegleria gruberi*	Heterolobosea	Protozoan	Joint Genome Institute DOE	V1.0	2006-10-23	2010-10-14
5722	*Trichomonas vaginalis*	Parabasalidea	Protozoan	TrichDB	V1.2	2010-09-21	2010-10-14
5741	*Giardia intestinalis*	Diplomonadida	Protozoan	GiardiaDB	V2.3 Assemblage A	2010-09-13	2010-10-15
5664	*Leishmania major*	Kinetoplastida	Protozoan	TriTrypDB	V2.4	2010-08-06	2010-10-14
185431	*Trypanosoma brucei* TREU 927	Kinetoplastida	Protozoan	TriTrypDB	V2.4	2010-08-06	2010-10-14

EMBL, European Molecular Biology Laboratory.

Table S4. Topology testing using Consel

Topology	AU	NP	BP	PP	KH	SH	WKH	WSH
Reported topology (RAxML)	0.775	0.741	0.741	0.736	0.758	0.81	0.758	0.791
Alternative topology 1	0.122	0.04	0.039	0.119	0.183	0.19	0.183	0.352
Alternative topology 2	0.303	0.219	0.221	0.145	0.242	0.242	0.242	0.371

AU, approximately unbiased test; BP, bootstrap probability; KH, Kishino–Hasegawa test; NP, nonparametric bootstrap probability; PP, Bayesian posterior probability; SH, Shimodaira–Hasegawa test; WKH, weighted Kishino–Hasegawa test; WSH, weighted Shimodaira–Hasegawa test.

Table S5. HMM-HMM comparisons using HHsearch between homologous BBSome subunits

Query/hit	BBS1	BBS2	BBS7	BBS9
BBS1	0	1.3×10^{-4}	7.3×10^{-7}	3.1×10^{-6}
BBS2	5.2×10^{-5}	0	1.8×10^{-28}	2.6×10^{-6}
BBS7	1.1×10^{-6}	2.4×10^{-26}	0	3.6×10^{-4}
BBS9	5×10^{-7}	1.2×10^{-6}	6×10^{-5}	0

HMM, hidden Markov model.